Biocatalytic Release of an Anticancer Drug from Nucleic-Acids-Capped Mesoporous SiO_2 Using DNA or Molecular Biomarkers as Triggering Stimuli

Zhanxia Zhang,[§,†] Dora Balogh,[§,†] Fuan Wang,[†] Sohn Yang Sung,[‡] Rachel Nechushtai,[‡] and Itamar Willner[†,*]

[†]Institute of Chemistry, Center for Nanoscience and Nanotechnology, The Hebrew University of Jerusalem, Jerusalem 91904, Israel and [‡]Department of Plant and Environmental Sciences, the Wolfson Centre for Applied Structural Biology, The Hebrew University of Jerusalem, Givat Ram 91904, Israel. [§]These authors contributed equally.

ABSTRACT DNA-gated mesoporous SiO_2 nanoparticles, MP-SiO_2 NPs, loaded with rhodamine B, RhB, act as "smart" materials that reveal complementary "sense" and "release" functionalities. The unlocking of the DNA pore-capping units is achieved by the biocatalytic cleavage of the DNA, and the unlocking process is amplified by the regeneration of the analyte-trigger. The RhB-loaded MP-SiO_2 NPs are capped with nucleic acid hairpin structures that lock the RhB in the pores. Opening of the hairpin structures by a nucleic acid analyte trigger or by the formation of an aptamer–substrate (ATP) complex leads to the formation of duplex structures being cleaved by exonuclease III, Exo III, or the nicking enzyme, Nb. BbvCI. This results in the regeneration of the target analytes, the autonomous unlocking of the pores, and the release of RhB. The systems reveal selectivity, and one-, two-, three-base mutations in the target DNA, or substitution of ATP with other triphosphate nucleotides, prohibit the unlocking of the pores. In analogy to the biocatalytic release of the model fluorophore substrates, the anticancer drug camptothecin, CPT, was entrapped in the pores and locked by the 1 or 11 hairpin structures. The drug was released from the pores in the presence of the nucleic acid 2 or ATP and the Exo III, as biocatalyst. Similarly, CPT locked in the pores by the 6 or 12 hairpins were released from the pores in the presence of ATP and Nb. BbvCI, as nicking enzyme, respectively. The effects of the CPT-loaded MP-SiO_2 NPs, capped with the ATP-dependent lock 6, on the viability of MDA-231 breast cancer cells and MCF-10a normal breast cells were examined. We find that after 48 h, 65% cell death was observed for the MDA-231 cancer cells, where only 25% cell death was observed for the normal cells. The higher cell death of the cancer cells correlates well with the enhanced metabolic synthesis of ATP in the cancerous cells.

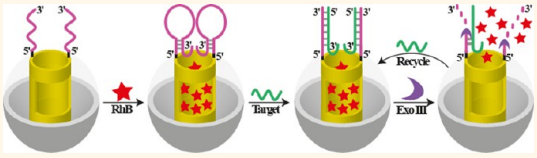

KEYWORDS: mesoporous SiO_2 · nanoparticle · controlled release · aptamer · exonuclease III · nicking enzyme

Mesoporous SiO_2 (MP-SiO_2) is a useful material due to its porous structure that allows the encapsulation of substrates and to the ability to modify its surface.[1] These properties of MP-SiO_2 were implemented to develop new catalysts,[2–4] drug delivery systems[5–7] and imaging materials.[8–10] The chemical modification of MP-SiO_2 enabled the design of stimuli-responsive MP-SiO_2 nanoparticles. Specifically, the capping of the pores that include entrapped substrates with stimuli-sensitive units enables the gating of the pores by the signal-triggered "unlocking" of the pores, and the controlled release of the entrapped substrate. Different external stimuli were applied to "unlock" the pores, including photonic signals,[11–13] redox signals,[14–16] pH,[17–19] and enzymes.[20–23] Furhtermore, supramolecular constructs, acting as molecular machines (valves), were assembled as capping units of the MP-SiO_2 pores, thus allowing the mechanical release of the entrapped material.[24,25]

Nucleic acids have been implemented as stimuli-responsive capping units of the pores associated with MP-SiO_2 nanoparticles (NPs).[26–28] Duplex DNA structures that included in one of the strands the adenosine 5′-triphosphate (ATP)-aptamer sequence were used to block the pores of MP-SiO_2. The formation of the ATP-aptamer complex released one of the strands, thus leading to the opening of the pores and the release of the entrapped substrate.[29] Similarly, pH-sensitive nucleic-acid-functionalized MP-SiO_2 nanoparticles (NPs) were prepared.[30]

* Address correspondence to willnea@vms.huji.ac.il.

Received for review April 22, 2013 and accepted August 28, 2013.

Published online August 28, 2013
10.1021/nn403772j

While the i-motif quadruplex structure of the capping nucleic acids, at pH = 5.2, locked the substrate in the pores, the dissociation of the i-motif structure at pH = 7.2 unlocked the pores and allowed the release of the substrate. In addition, thymine-Hg^{2+}-thymine bridged nucleic acid duplexes were implemented to block the pores of MP-SiO_2 NPs, and the removal of the bridging nucleic acid released the pore-entrapped substrate.[31]

The photonically driven opening of nucleic acid capped MP-SiO_2 NPs was also reported.[32] By one approach, the pH changes stimulated by the irradiation of a triphenylcarbinol photoactive compound was used to dissociate i-motif-capped MP-SiO_2 NPs and release the entrapped substrate. By a second approach, photoisomerizable *trans*-azobenzene units were used to cooperatively stabilize duplex DNA structures that cap the pores of the MP-SiO_2 NPs. Photoisomerization to the *cis*-azobenzene state decreased the stability of the duplex DNA structure, resulting in their dissociation, the pore opening and the release of the entrapped substrate.[33] Besides the opening of the pores of the nucleic-acid-capped MP-SiO_2 NPs with chemical or photonic signals, biocatalytic transformations of the fragment of the nucleic acid capping units were also implemented to lock and open the pores. For example, deoxyribonuclease hydrolysis of duplex DNA capping units was used to open the pores.[34] Recently, DNAzyme−substrate complexes were used to lock the pores of the MP-SiO_2 NPs and release the substrates upon the addition of the DNAzyme cofactor, *e.g.*, Mg^{2+} or Zn^{2+} ions.[35] In all of these catalytic systems, the stimulated opening of the pores and the release of the substrates proceeded as a passive reaction. It would be a major advance if one could design gated systems, where the biocatalytic process is activated by a primary sensing or recognition event of an analyte or biomarker of particular interest, and where the biocatalytic process recycles and regenerates the analyte. Such systems could release a substrate (drug), as a result of detection of minute amounts of biomarkers.

In the present study, we describe the gating of the pores of MP-SiO_2 NPs with functional nucleic acids and the unlocking of the pores by a coupled recognition/biocatalytic effect. The recognition events of an analyte (biomarker) transform the capping element into a new functional element that undergoes biocatalytic scission. The scission process fragments a part of the capping unit and releases the analyte biomarker for the further autonomous catalytic degradation of the capping element, thus unlocking the pores and allowing the release of the pore-entrapped material. Thus, we present here the assembly of "smart" model materials that sense biomarkers that trigger the autonomous biocatalytic unlocking of the pores and the release of substrates (analogs for drugs) from the pore containers. The biocatalytic regeneration of the biomarkers provides an amplification mechanism where a low amount of the biomarkers allows the release of high content of the entrapped substrate (drug).

RESULTS

Aminopropylsiloxane-MP-SiO_2 NPs (300 nm in diameter, as shown in Figure S1 (Supporting Information)) were prepared according to the reported method.[30] The mesoporous materials exhibited a surface area corresponding to 733 m^2/g, an average pore diameter of 2−3 nm and average pore volume of 0.19 cm^3/g, as shown in Figure S2 (Supporting Information).

Figure 1A depicts a coupled sensing/biocatalytic unlocking process that implements nucleic acid functionalized MP-SiO_2 NPs and exonuclease III, Exo III,[36−38] as biomarker regeneration biocatalyst. Exo III requires for its biocatalytic activity a duplex structure, and it hydrolytically digests the 3′-end of the duplex DNA structure. Accordingly, the 5′-end of the nucleic acid (**1**) was covalently linked to amine-functionalized MP-SiO_2 NPs using sulfo-EMCS as covalent cross-linker. The nucleic acid **1** includes a tailored base sequence that generates at room temperature a hairpin structure that includes a single-stranded loop for the recognition of a nucleic acid biomarker. The hairpin structure reveals, however, a low melting temperature (67.3 °C) and, thus, exists at higher temperatures in a random coil single-stranded configuration, and at room temperature (25 °C), it folds to the energetically stabilized hairpin structure. Thus, the pores of the MP-SiO_2 are loaded with rhodamine B, RhB, as fluorescent dye, at 90 °C, where the nucleic acid **1** is in the random coil configuration. The system was then allowed to cool to 25 °C, where **1** folds into the hairpin structure. Figure S3 (Supporting Information) depicts the images of the MP-SiO_2 before and after loading with RhB. The MP-SiO_2 NPs loaded with RhB are colored with the dye, but the fluorescent dye is nonremovable, implying that the dye is, indeed, trapped in the pores. The results following the washing of the MP-SiO_2 NPs and the removal of any fluorescent dye linked to the exterior region outside the pores are shown in Figure S4 (Supporting Information). Treatment of the **1**-capped MP-SiO_2 NPs with the analyte (biomarker) nucleic acid **2** results in the opening of the hairpin to form a duplex structure. The 3′-end of the duplex structure is hydrolytically "digested" by Exo III, resulting in the shortage of **1** and the release of the analyte (biomarker) strand (**2**). The latter strand opens a further hairpin structure and leads to the subsequent cleavage of the resulting duplex through the digestion of the 3′-end. That is, the analyte (biomarker) is sensed by the hairpin structure, and it triggers the autonomous Exo III regeneration of the analyte and the unlocking of the pores, while releasing RhB. Note that the analyte (biomarker) strand, **2**, is not affected by Exo III, since it includes a single-stranded 3′-ended nucleic acid tether. Figure 1B shows the fluorescence intensities of the released RhB,

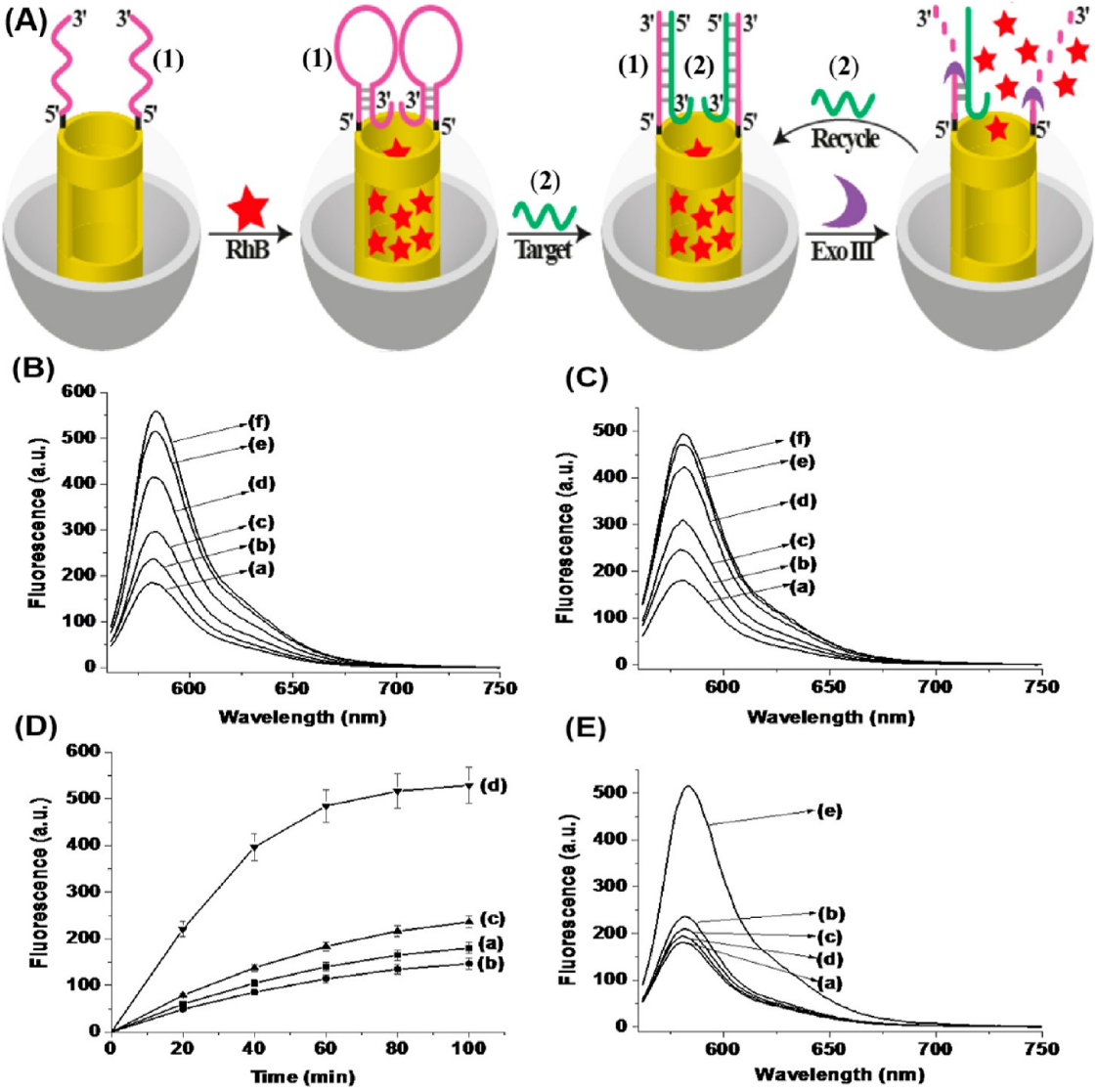

Figure 1. (A) Unlocking of hairpin-capped mesoporous SiO_2 NPs and the release of rhodamine B, RhB, using an analyte–DNA biomarker (2) as activator for opening the hairpins and implementing Exo III as biocatalyst for the regeneration of the DNA–biomarker. (B) Fluorescence spectra corresponding to the release of RhB upon subjecting the MP-SiO_2 NPs (10 mg) to different concentrations of the biomarker analyte in the presence of Exo III (1 U/μL), for a fixed time interval of 60 min: (a) 0 nM; (b) 50 nM; (c) 100 nM; (d) 500 nM; (e) 1 μM; (f) 2.5 μM. (C) Fluorescence spectra corresponding to the release of RhB upon subjection of the MP-SiO_2 NPs (10 mg) to different concentrations of Exo III in the presence of a constant concentration of 2 (1 μM), for a fixed time interval of 60 min: (a) 0 U/μL; (b) 0.05 U/μL; (c) 0.1 U/μL; (d) 0.5 U/μL; (e) 1 U/μL; (f) 2 U/μL. (D) Time-dependent fluorescence changes observed upon the release of RhB from the MP-SiO_2 NPs by: (a) the RhB-loaded system without treatment with the biomarker (2) or Exo III; (b) treatment of the RhB-loaded system only with the biomarker–DNA, 2, (1 μM) without adding Exo III; (c) treatment of the RhB-loaded system only with Exo III (1 U/μL) and without the addition of (2); (d) treatment of the RhB-loaded MP-SiO_2 NPs with 2 (1 μM) and Exo III (1 U/μL). (E) Fluorescence spectra of the release RhB upon treatment of the hairpin-locked, RhB-loaded MP-SiO_2 NPs with: (a) no DNA–biomarker; (b–d) treatment with the one-, two-, three-base mutants DNA biomarker 3, 4, and 5, respectively, each 1 μM; (e) treatment with 2 (1 μM). In all experiments, Exo III (1 U/μL) was included in the systems, and the fluorescence spectra were recorded after a fixed time interval of 60 min.

after a fixed time interval of 60 min, and in the presence of 1 U/μL Exo III, using different concentrations of the analyte–biomarker to trigger the opening of the pores. As the concentration of the analyte–biomarker increases, the content of the released dye within the time interval of 60 min is higher, consistent with the increase in primary opening of the hairpins by **2** that triggers the regeneration of the target–biomarker and the Exo III-stimulated opening of the pores. Similarly, Figure 1C shows the fluorescence intensities of the released RhB in the presence of the **1**-capped MP-SiO_2 NPs, and a fixed concentration of the analyte–biomarker **2**, 1 μM, upon treatment with different concentrations of Exo III for a fixed time interval of 60 min. Evidently, as the concentration of Exo III increases, the amount of the released RhB is higher, consistent with the enhanced opening of the hairpin-locked MP-SiO_2 NPs by the autonomous Exo III regeneration of the

target biomarker units. Figure 1D shows the rate of release of RhB from several control systems that include the RhB-entrapped MP-SiO_2 NPs. The entrapped RhB leaks out from the hairpin-capped pores even in the absence of the target analyte–biomarker, curve a. The leakage of RhB is very similar in the presence of only the target or the Exo III, curves b and c, respectively. The rapid release of RhB proceeds only in the presence of the analyte target (1 μM) and Exo III (1 U/μL), curve d. After 60 min the released RhB reaches a saturation value. Using an appropriate calibration curve, we estimated that the released amount of RhB was *ca.* 8.5 μmol/g MP-SiO_2 NPs. The release process of RhB from the MP-SiO_2 NPs is, also, very sensitive to the primary sensing of the biomarker–analyte. Figure 1E shows that one-, two-, or three-base mutations in the target–biomarker, strands **3**, **4**, and **5**, respectively, do not open the hairpin-capping units and do not activate the Exo III autonomous cleavage of the capping units. The release of the RhB using **3**, **4**, or **5** as analyte–biomarkers, and in the presence of Exo III, proceeds inefficiently and is very similar to the background leakage of RhB from the channels, Figure 1D, curves a, b, and c.

A further biocatalytically stimulated opening of hairpin–nucleic-acid-capped pores of MP-SiO_2, and the release of the entrapped substrate, is described in Figure 2A. The MP-SiO_2 NPs are functionalized with the nucleic acid **6** by covalently binding the 5′-end of the nucleic acid to the amine-functionalized MP-SiO_2 NPs, using sulfo-EMCS as cross-linker. At 90 °C, **6** exists as a single-stranded chain, while at 25 °C, the chain stabilizes into a hairpin structure. Thus, the pores of the MP-SiO_2 NPs are loaded with RhB at 90 °C and the cooling of the system results in the hairpin-locked RhB in the pores. The interaction of the hairpin-capped pores with the analyte–biomarker **7** results in the formation of the duplex structure **6**/**7** that still acts as a structural stopper of the pores. Nonetheless, the duplex structure **6**/**7** is tailored in such a way that it includes the programmed duplex sequence for the specific nicking of one base in the duplex.[39−41] Nicking of strand **6** leads to the separation of an unstable duplex structure that dissociates and regenerates the analyte–biomarker (**7**) for a secondary opening of a hairpin and nicking of the resulting duplex stopper. Note that the hairpin, generated by the folding of **6**, does not include the appropriate duplex domain for being nicked, and this domain is formed only upon the hybridization of the analyte–biomarker with the single-stranded sensing loop of the hairpin. Thus, the hybridization of the analyte–biomarker with the hairpin capping units triggers the nicking of the pore-gating units and the regeneration of the analyte–biomarker for the autonomous release of the capping units and the subsequent release of the entrapped substrate (RhB). The rate of release of RhB is controlled by the concentration of the analyte–biomarker **7** that opens the locking hairpin capping units. Figure 2B depicts the fluorescence intensities of the released RhB upon treatment of the **6**-capped MP-SiO_2 NPs with variable concentrations of the analyte–biomarker, for a fixed time interval of 60 min and a constant amount of the Nb. BbvCI nicking enzyme corresponding to 0.5 U/μL. As the concentration of the analyte–biomarker increases, the fluorescence of the released RhB is intensified, consistent with a higher degree of opening of the hairpin capping units that enhances the opening of the pores by the autonomous nicking/analyte regeneration process. Similarly, at a fixed concentration of the analyte–biomarker, the release of RhB from the pores is controlled by the concentration of the Nb. BbvCI nicking enzyme. Figure 2C shows the fluorescence intensities of the released RhB, upon treatment of the **6**-capped RhB-loaded MP-SiO_2 NPs with a constant concentration of the analyte–biomarker, 1 μM, for a fixed time interval of 60 min, in the presence of variable amounts of the nicking enzyme. As the content of the enzyme increases, the amount of released RhB is higher, consistent with the enhanced opening of the pores through the autonomous biocatalytic cleavage of the capping units and the regeneration of the analyte–biomarker. In the presence of 0.5 U/μL of the nicking enzyme, the fluorescence intensity of the system reaches a saturation value, implying that under these conditions, most of the RhB was removed from the mesoporous matrix. Control experiments, Figure 2D, reveal that when the **6**-capped pores are not interconnected with the nicking enzyme or the analyte–biomarker, the leakage of RhB is observed, curve a, and the analyte–biomarker or the nicking enzyme alone has little effect on the release of RhB, curves b and c, respectively. Curve d of Figure 2D shows the time-dependent fluorescence spectra of the solution, upon the treatment of the **6**-hairpin-locked MP-SiO_2 NPs that include entrapped RhB, with the analyte–biomarker **7**, 1 μM, in the presence of the nicking enzyme, 0.5 U/μL. The effective release of RhB from the pores proceeds only when the **6**-hairpin blocked pores are reacted with the analyte–biomarker and the nicking enzyme. A time-controlled release of RhB is observed in curve d that tends to reach a saturation value after *ca.* 60 min. From the saturated value of the fluorescence spectrum, and using an appropriate calibration curve, we estimated that the released amount of RhB was *ca.* 12.4 μmol/g MP-SiO_2 NPs. Further support that the hybridization of **7** to the hairpin-**6**-modified MP-SiO_2 NPs leads to a duplex structure being nicked by Nb. BbvCI, and the unlocking of the pores through the release of the fragmented capping units was obtained by gel electrophoresis experiments that followed the fragmented product, Figure S6 (Supporting Information). Also, the opening of the **6**-modified pores by the coupled opening of

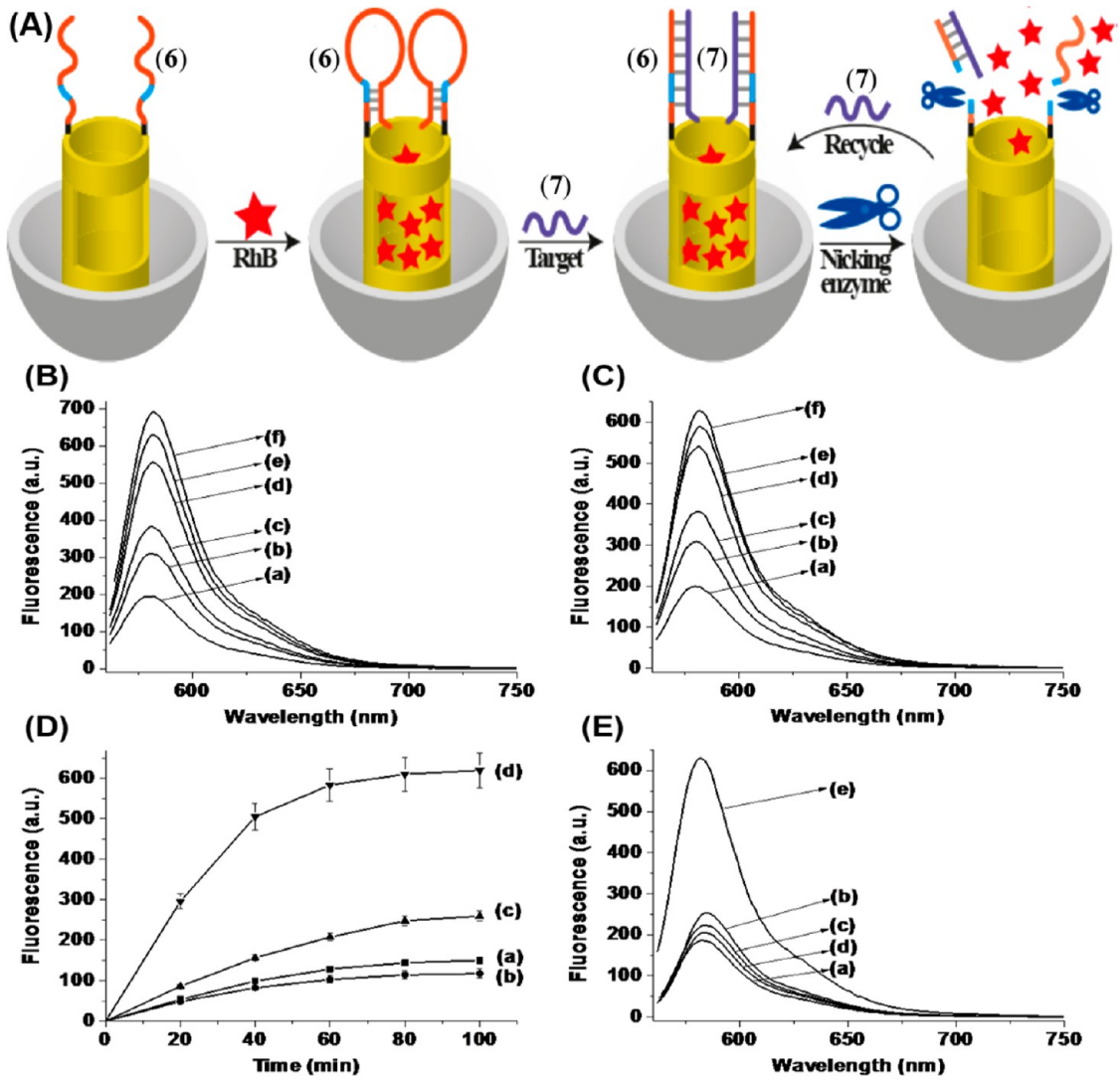

Figure 2. (A) Unlocking of hairpin-capped mesoporous SiO_2 NPs and the release of rhodamine B, RhB, using an analyte–DNA biomarker (7) as activator for opening the hairpins and implementing a Nb. BbvCI nicking enzyme as biocatalyst for the regeneration of the DNA–biomarker. (B) Fluorescence spectra corresponding to the release of RhB upon subjecting the MP-SiO_2 NPs (10 mg) to different concentrations of the biomarker analyte in the presence of the Nb. BbvCI nicking enzyme (0.5 U/μL), for a fixed time interval of 60 min: (a) 0 nM; (b) 50 nM; (c) 100 nM; (d) 500 nM; (e) 1 μM; (f) 2.5 μM. (C) Fluorescence spectra corresponding to the release of RhB upon subjecting the MP-SiO_2 NPs (10 mg) to different concentrations of the Nb. BbvCI nicking enzyme in the presence of a constant concentration of 7 (1 μM), for a fixed time interval of 60 min: (a) 0 U/μL; (b) 0.05 U/μL; (c) 0.1 U/μL; (d) 0.5 U/μL; (e) 1 U/μL; (f) 2 U/μL. (D) Time-dependent fluorescence changes observed upon the release of RhB from the MP-SiO_2 NPs by: (a) the RhB-loaded system without treatment with the biomarker 7 or nicking enzyme; (b) treatment of the RhB-loaded system only with the biomarker–DNA, 7, (1 μM) without adding nicking enzyme; (c) treatment of the RhB-loaded system only with nicking enzyme (0.5 U/μL) and without the addition of 7; (d) treatment of the RhB-loaded MP-SiO_2 NPs with 7 (1 μM) and nicking enzyme (0.5 U/μL). (E) Fluorescence spectra of the release RhB upon treatment of the hairpin-locked, RhB-loaded MP-SiO_2 NPs with: (a) no DNA–biomarker; (b–d) treatment with the one-, two-, three-base mutants DNA biomarker 8, 9, and 10, respectively, each 1 μM; (e) treatment with 7 (1 μM). In all experiments, the Nb. BbvCI nicking enzyme (0.5 U/μL) was included in the systems, and the fluorescence spectra were recorded after a fixed time interval of 60 min.

the hairpins by means of the analyte–biomarker and the autonomous nicking of the capping units, by means of the precise nicking recognition sites (CCTCAGC/GGAGT$_{\blacktriangle}$CG), reveals impressive selectivity, Figure 2E. One-base, two-base, or three-base mismatches in the analyte–biomarker, sequences **8**, **9**, and **10**, respectively, do not open the hairpin structure, and the autonomous biocatalytic removal of the capping units by the nicking enzyme is prohibited. Thus, in the presence of the mutants, the release of RhB from the pores is very similar to the intrinsic leakage of the dye from the **6**-functionalized pores, Figure 2D, curves a, b, and c, respectively.

In the previous systems, the opening of the nucleic-acid-functionalized pores was triggered by nucleic acid analyte–biomarker strands, where biocatalytic reactions, stimulated by Exo III or the nicking enzymes, provided means to remove the capping elements,

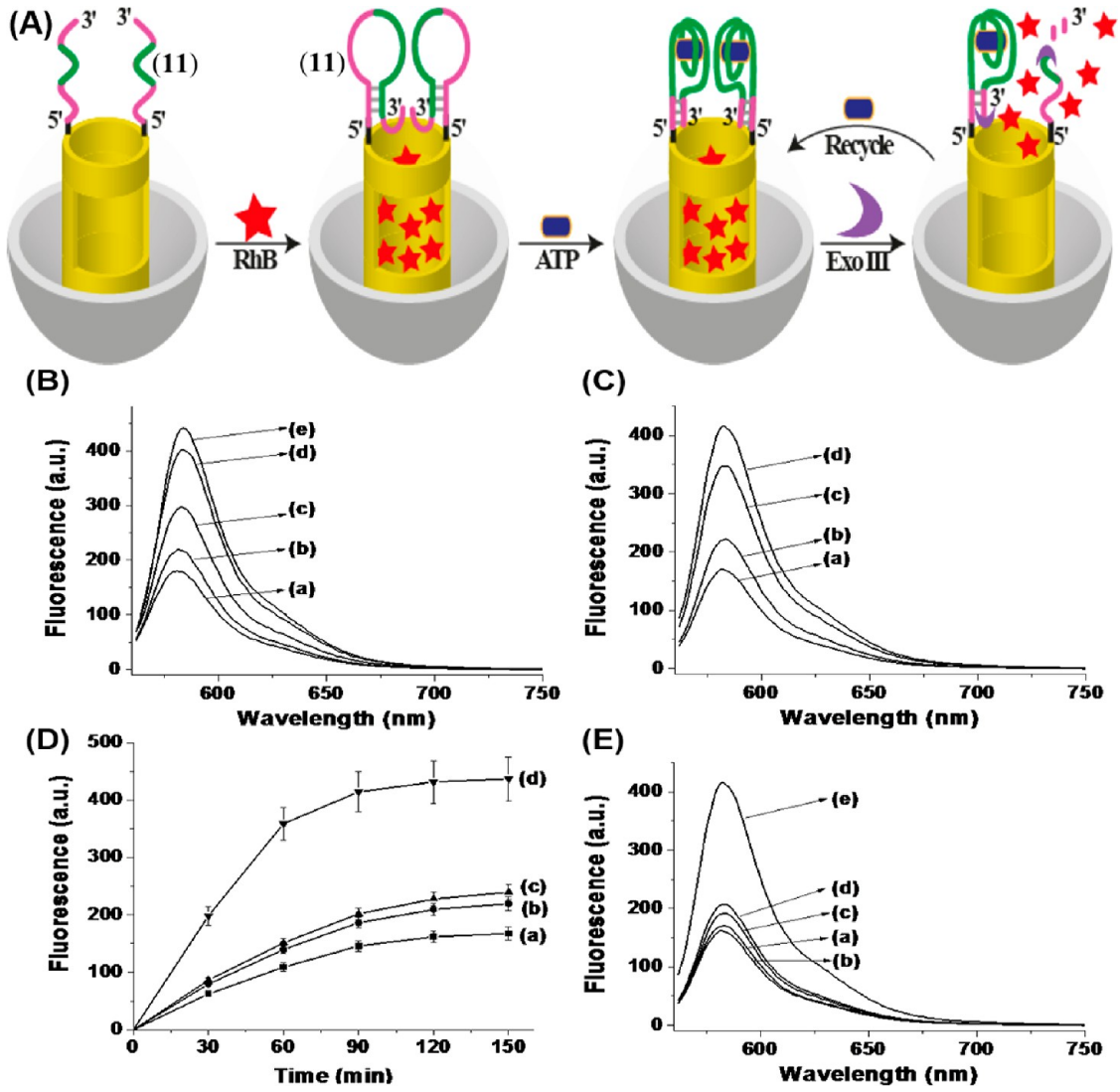

Figure 3. (A) Unlocking of hairpin-gated MP-SiO_2 NPs and the release of RhB by the opening of the hairpin gating units through the formation of ATP−aptamer complex, while regenerating the ATP-biomarker with Exo III. (B) Fluorescence spectra corresponding to the release of RhB upon treatment of the hairpin-protected, RhB-loaded, MP-SiO_2 NPs with variable concentrations of ATP in the presence of Exo III (1 U/μL), for a fixed time interval of 90 min: (a) 0 μM; (b) 100 μM; (c) 500 μM; (d) 1 mM; (e) 2 mM. (C) Fluorescence spectra corresponding to the release of RhB from the RhB-loaded MP-SiO_2 NPs upon treatment with variable concentrations of Exo III, and a constant concentrations of ATP (1 mM), for a fixed time interval of 90 min: (a) 0 U/μL; (b) 0.1 U/μL; (c) 0.5 U/μL; (d) 1 U/μL. (D) Time-dependent fluorescence changes upon treatment of the RhB-loaded MP-SiO_2 NPs: (a) with no ATP and no Exo III; (b) in the presence of only ATP (1 mM), without Exo III; (c) in presence of Exo III (1 U/μL) without ATP; (d) in the presence of ATP (1 mM) and Exo III (0.5 U/μL). (E) Selectivity studies demonstrating the specific unlocking of the pores by ATP. Fluorescence spectra corresponding to the release of RhB from the RhB-loaded MP-SiO_2 NPs: (a) in the absence of ATP; (b−d) in the presence of UTP, GTP, CTP, each 1 mM, respectively; (e) in the presence of ATP (1 mM). All fluorescence spectra were recorded in the presence of Exo III (1 U/μL), and after a fixed time interval of 90 min.

while regenerating the biomarker units. This concept was further developed to open the pores and release the entrapped substrate (RhB) by means of aptamer−substrate complexes and the coupled autonomous biocatalytic degradation of the aptamer−substrate complex, while regenerating the substrate−biomarker. One configuration for the controlled release of RhB from the MP-SiO_2 NPs pores by the coupled ATP−aptamer complex and Exo III biocatalytic process is depicted in Figure 3A. The nucleic acid **11**, modifying the MP-SiO_2 NPs, exists at 90 °C in the random coil structure, thus allowing the loading of the pores with RhB. The pores with the entrapped RhB are capped by the hairpin structures that are stabilized at 25 °C. The hairpin structures of **11** are designed to include an aptamer sequence (green), and this is conjugated to a single-stranded sequence (pink), which ensures that Exo III cannot hydrolytically affect the hairpin structures. In the presence of ATP, the hairpin **11** opens, and the 3′-end of the opened hairpin is designed to form a duplex structure with the 5′-domain of **11**. That is, the generated ATP−aptamer

complex is cooperatively stabilized by this duplex domain. The resulting duplex provides, however, an active site for the Exo III-stimulated hydrolytic digestion of the 3′-end of the duplex. This biocatalytic process destabilizes the ATP–aptamer complex that releases ATP for a secondary opening of a hairpin structure, which yields the aptamer–ATP complex. Thus, opening of the hairpin by ATP triggers the coupled Exo III-stimulated regeneration of ATP for the autonomous biocatalytic "digestion" of the capping units, and the release of the entrapped RhB. Figure 3B depicts the fluorescence spectra of the RhB released from the pores, upon treatment of the MP-SiO_2 NPs with different concentrations of ATP, for a fixed time interval of 90 min, and using a constant concentration of Exo III, corresponding to 1 U/μL. Similarly, Figure 3C shows the fluorescence spectra of RhB released from the MP-SiO_2 NPs upon treatment of the NPs with different concentrations of Exo III and a constant concentration of ATP (1 mM), for a fixed time interval of 90 min. The release of RhB from the porous material is enhanced either by increasing the concentration of ATP or the concentration of Exo III, consistent with the fact that these two ingredients control the opening of the capping units of the pores. Figure 3D shows a set of control experiments that were performed to elucidate the functions of ATP and Exo III on the controlled release of RhB from the pores. In the absence of ATP or Exo III, leakage of RhB from the pores is observed, curve a. In the presence of either ATP or Exo III, a similar leakage rate of RhB is observed, curves b and c, respectively. The enhanced release of RhB is detected only in the presence of ATP, 1 mM, and Exo III, 1 U/μL, curve d, consistent with the suggested, mechanism, where the opening of the **11**-functionalized pores, to yield the respective aptamer–substrate complex, is coupled to the autonomous cleavage of the capping units, and the regeneration of the ATP analyte–biomarker. Using the appropriate calibration curve, we estimated that the released amount of RhB was *ca.* 9.3 μmol/g MP-SiO_2 NPs. Finally, the controlled opening of the **11**-functionalized MP-SiO_2 NPs is selective for ATP, and other nucleotides (UTP, GTP, CTP) do not affect the opening of the pores, Figure 3E.

In analogy to the coupled nucleic acid/nicking enzyme catalysed opening of the pores, we have implemented the aptamer–substrate complex/nicking enzyme method, to drive the autonomous opening of the pores for the controlled release of RhB, Figure 4A. The MP-SiO_2 NPs were modified with **12** and loaded with RhB at 90 °C. Upon cooling of the system to 25 °C, the single-strand stabilizes the hairpin structures that cap the RhB in the pores. The stem-region of the hairpin does not include the sequence-specific domain to be nicked by the Nb. BbvCI nicking recognition sites (CCTCAGC/GGAGT$_{\blacktriangle}$CG). The formation of the ATP–aptamer complex rearranges the hairpin structure to a new structure that includes the nicking domain. The fragmentation of the stem region of the ATP–aptamer complex releases a major fragment of the aptamer sequence, resulting in the release of ATP from the fragmented sequence. The recycled ATP biomarker opens all additional hairpin capping units, thus triggering the autonomous opening of the pores and the release of RhB, by the cyclic coupled opening of the hairpin units by ATP, formation of the ATP-aptamer complex, the subsequent nicking enzyme-stimulated fragmentation (GGAGT$_{\blacktriangle}$CG) of the aptamer sequence and the recycling of the ATP biomarker. Figure 4B shows the fluorescence spectra of the released RhB upon the treatment of the **12**-capped RhB-loaded MP-SiO_2 NPs, and a constant concentration of the nicking enzyme, 0.5 U/μL, in the presence of variable concentrations of ATP, for a fixed time interval of 90 min. As the concentration of ATP increases, the fluorescence intensities of the released RhB are intensified. These results are consistent with the fact that as the concentration of ATP is higher, the autonomous opening of the pores through the concentration of ATP is higher, and the coupled formation of the ATP–aptamer complex and its fragmentation by the nicking enzyme are enhanced. Figure 4C shows the fluorescence intensities of the released RhB, upon treatment of the RhB-loaded MP-SiO_2 NPs with a fixed concentration of ATP, 1 mM, and variable concentrations of the Nb. BbvCI nicking enzyme, for a fixed time interval of 90 min. As the concentration of the nicking enzyme increases, the release of RhB is higher, consistent with the enhanced opening of the pores. Figure 4D shows the time-dependent fluorescence changes upon the release of RhB, by the coupled ATP/nicking enzyme opening of the pores, in comparison to control systems. While the **12**-modified MP-SiO_2 NPs reveal an intrinsic leakage of RhB, curve a, the leakage process in the presence of only ATP or the nicking enzyme is only slightly affected, curves b and c, respectively. Only the combination of ATP, 1 mM, and the Nb. BbvCI nicking enzyme, 0.5 U/μL, yields a substantial enhancement in the release of RhB, curve d, consistent with the suggested mechanism. Using the calibration curve, we estimated that the released amount of RhB was *ca.* 14.1 μmol/g MP-SiO_2 NPs. Figure 4E reveals the selective ATP-triggered release of RhB from the **12**-functionalized MP-SiO_2 NPs, using the respective ATP–aptamer complex and the nicking enzyme as biocatalyst. The release of RhB in the presence of the nucleotides CTP, UTP and GTP is very similar to the intrinsic leakage of RhB from the MP-SiO_2 NPs that is observed in the absence of ATP/nicking enzyme, Figure 4D, curves a–c as compared to curve d.

The study was further extended by demonstrating that the nucleic-acid-triggered or ATP-triggered release of the anticancer drug camptothecin, CPT, can be stimulated by the exonuclease III or the nicking enzyme, Nb. BbvCI, mediated unlocking of the pores.

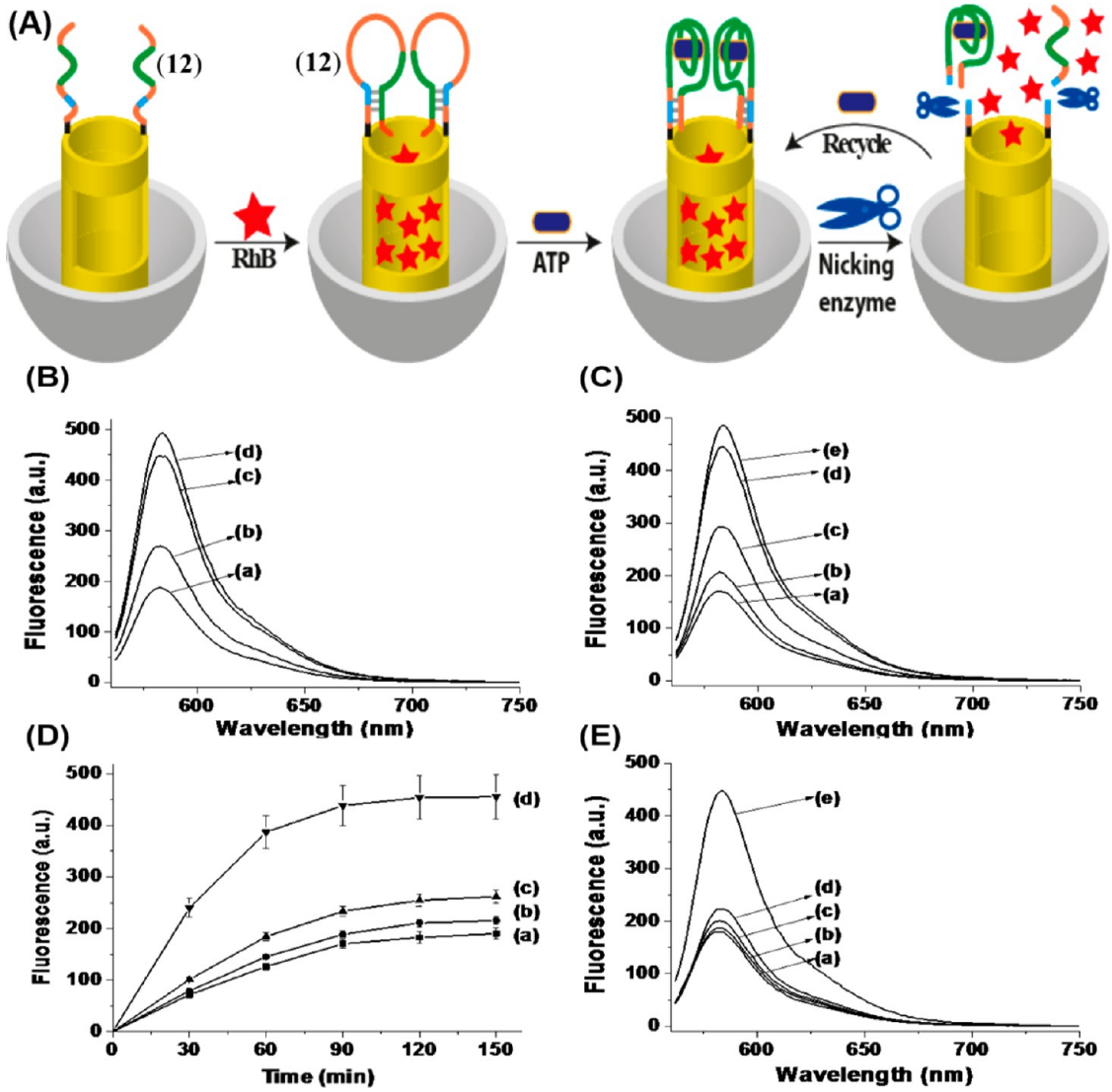

Figure 4. (A) Unlocking of hairpin-gated MP-SiO_2 NPs and the release of RhB by the opening of the hairpin gating units through the formation of ATP−aptamer complex, while regenerating the ATP−biomarker with a Nb. BbvCI nicking enzyme. (B) Fluorescence spectra corresponding to the release of RhB upon treatment of the hairpin-protected, RhB-loaded, MP-SiO_2 NPs with variable concentrations of ATP in the presence of the Nb. BbvCI nicking enzyme (0.5 U/μL), for a fixed time interval of 90 min: (a) 0 μM; (b) 100 μM; (c) 500 μM; (d) 1 mM; (e) 2 mM. (C) Fluorescence spectra corresponding to the release of RhB from the RhB-loaded MP-SiO_2 NPs upon treatment with variable concentrations of the Nb. BbvCI nicking enzyme, and a constant concentrations of ATP (1 mM), for a fixed time interval of 90 min; (a) 0 U/μL; (b) 0.1 U/μL; (c) 0.5 U/μL; (d) 1 U/μL. (D) Time-dependent fluorescence changes upon treatment of the RhB-loaded MP-SiO_2 NPs: (a) with no ATP and no nicking enzyme; (b) in the presence of only ATP (1 mM), without nicking enzyme; (c) in presence of nicking enzyme (0.5 U/μL) without ATP; (d) in the presence of ATP (1 mM) and nicking enzyme (0.5 U/μL). (E) Selectivity studies demonstrating the specific unlocking of the pores by ATP. Fluorescence spectra corresponding to the release of RhB from the RhB-loaded MP-SiO_2 NPs: (a) in the absence of ATP; (b−d) in the presence of CTP, UTP, GTP, each 1 mM, respectively; (e) in the presence of ATP (1 mM). All fluorescence spectra were recorded in the presence of the Nb. BbvCI nicking enzyme (0.5 U/μL), and after a fixed time interval of 90 min.

Furthermore, we describe the effective intracellular release of CPT in breast cancer cells, and we compare the effectiveness of unlocking pores and releasing CPT in breast cancer cells and normal breast cells and the effect on cell death in these cells. Figure 5A shows the fluorescence intensities of the released CPT, upon the treatment of CPT-**1**-lock MP-SiO_2 NPs with different concentrations of the target DNA, **2**, in the presence of Exo III for a fixed time interval of 60 min. As the concentration of the target DNA increases, the fluorescence is intensified, implying that more CPT was released from the pores. Figure 5B depicts the time-dependent fluorescence changes upon releasing CPT from the **1**-locked MP-SiO_2 NPs. The respective control experiments are shown in Figure 5B, curves a−c. Evidently, effective release of CPT is observed only upon unlocking of the pores with **2** and the Exo III degradation of the locking sites, curve d. Similar results are observed upon releasing CPT from the **6**-locked MP-SiO_2 NPs using the target DNA **7** and the nicking enzyme Nb. BbvCI, as opening mechanism, Figures 5C and D. In analogy, the ATP-stimulated opening and the

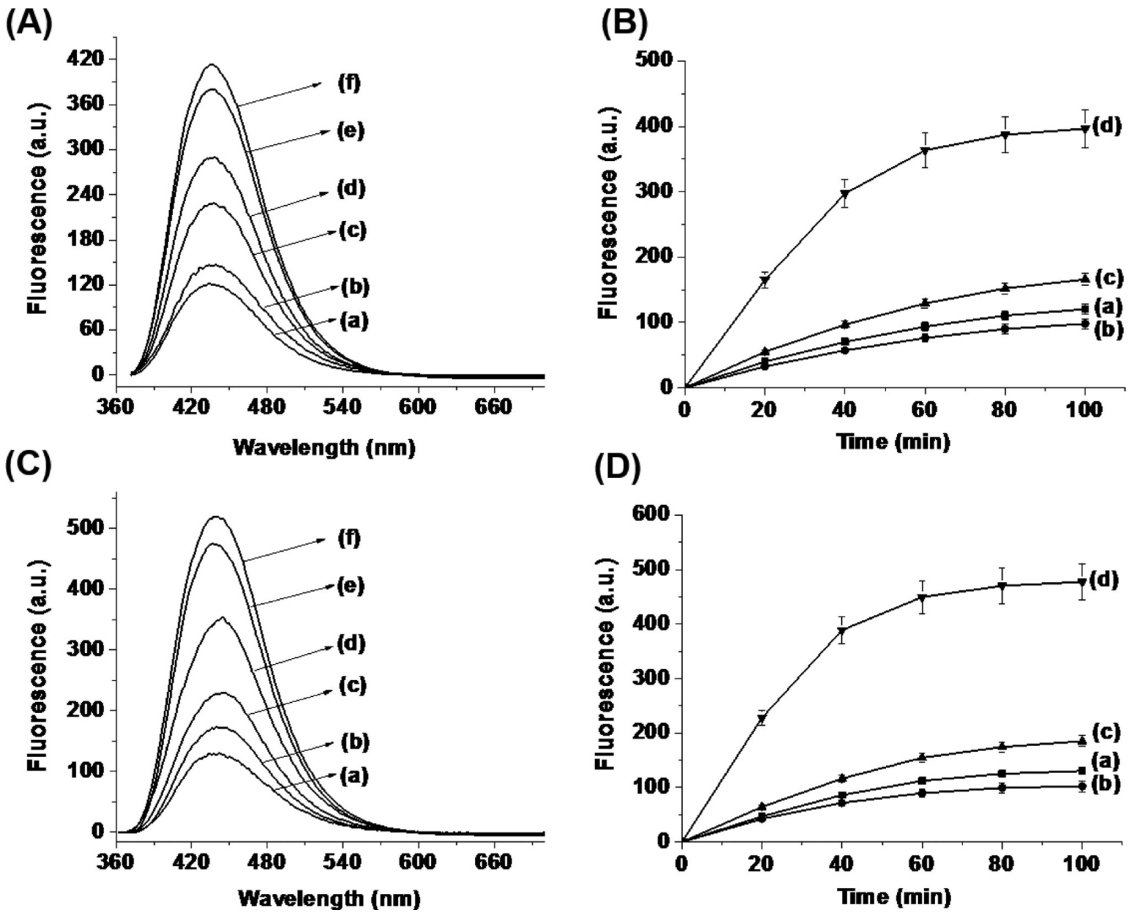

Figure 5. (A) Fluorescence spectra corresponding to the release of CPT upon subjecting the (1)-capped MP-SiO_2 NPs (10 mg) to different concentrations of the biomarker analyte in the presence of Exo III (1 U/μL), for a fixed time interval of 60 min: (a) 0 nM; (b) 50 nM; (c) 100 nM; (d) 500 nM; (e) 1 μM; (f) 2.5 μM. (B) Time-dependent fluorescence changes observed upon the release of CPT from the MP-SiO_2 NPs by: (a) the CPT-loaded system without the biomarker 7 or Exo III; (b) treatment of the CPT-loaded system only with the biomarker 7 (1 μM), without Exo III; (c) treatment of the CPT-loaded system only with Exo III (1 U/μL) and without 7; (d) treatment of the CPT-loaded MP-SiO_2 NPs with 7 (1 μM) and Exo III (1 U/μL). (C) Fluorescence spectra corresponding to the release of CPT upon subjecting the MP-SiO_2 NPs (10 mg) to different concentrations of the biomarker analyte in the presence of the Nb. BbvCI nicking enzyme (0.5 U/μL), for a fixed time interval of 60 min: (a) 0 nM; (b) 50 nM; (c) 100 nM; (d) 500 nM; (e) 1 μM; (f) 2.5 μM. (D) Time-dependent fluorescence changes observed upon the release of CPT from the MP-SiO_2 NPs by: (a) the CPT-loaded system without the biomarker 2 or nicking enzyme; (b) treatment of the CPT-loaded system only with the biomarker 2 (1 μM), without nicking enzyme; (c) treatment of the CPT-loaded system only with nicking enzyme (0.5 U/μL) and without the biomarker 2); (d) treatment of the CPT-loaded MP-SiO_2 NPs with 2 (1 μM) and nicking enzyme (0.5 U/μL).

release of CTP from the pores in the presence of Exo III or the nicking enzyme were studied. Figure 6A shows the fluorescence spectra observed upon the treatment of **11**-capped MP-SiO_2 NPs that included in-pore trapped CPT with different concentrations of ATP and Exo III, for a fixed time interval of 90 min. As the concentration of ATP increases, the amount of the released CPT is higher, consistent with the enhanced release of CPT from the pores. Using the appropriate calibration curve, we estimate that *ca.* 10.8 μmol/g MP-SiO_2 NPs of CPT are released, after a time interval of 90 min. Figure 6B depicts the time-dependent fluorescence changes upon releasing CPT from the **11**-capped MP-SiO_2 NPs. Similarly, Figures 6C and D show the release of CPT from the **12**-locked pores of the MP-SiO_2 NPs, using ATP as modifier of the "locker-keys" through the formation of the respective ATP–aptamer capping units, and the opening of the pores by the nicking-enzyme degradation of the ATP–aptamer complexes. As the concentration of the ATP increases, the release of CPT is enhanced, consistent with the increase in the content of the aptamer–ATP complexes, and their digestion by the nicking enzyme, Nb. BbvCI. The rate of release of the CPT from the pores in the respective control experiments, Figure 6D, curves a–c, and in the presence of the nicking enzyme, Figure 6D, curve d, indicate that the CPT trapped in the **12**-locked pores is effectively released only in the presence of the biomarker and the nicking enzyme. From the respective calibration curve, we estimated that *ca.* 13.4 μmol/g MP-SiO_2 NPs were released from the pores after a time interval of *ca.* 90 min.

The concept to unlock and release CPT from the pores of the MP-SiO_2 NPs by transforming the "locker-keys" with DNA or ATP biomarkers into new functional

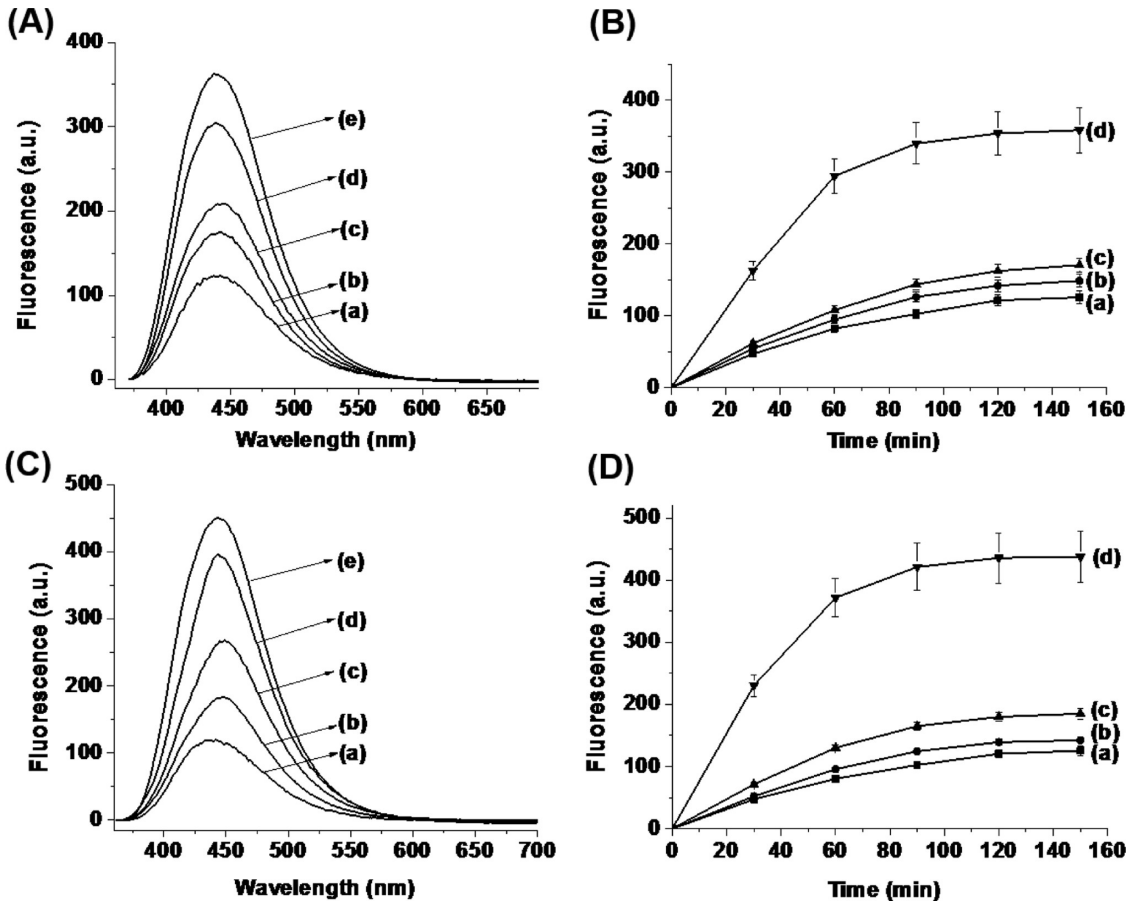

Figure 6. (A) Fluorescence spectra corresponding to the release of CPT upon treatment of the 11-capped MP-SiO_2 NPs with variable concentrations of ATP, in the presence of Exo III (1 U/μL), for a fixed time interval of 90 min; (a) 0 μM; (b) 100 μM; (c) 500 μM; (d) 1 mM; (e) 2 mM. (B) Time-dependent fluorescence changes upon treatment of the CPT-loaded MP-SiO_2 NPs: (a) with no ATP and no Exo III; (b) in the presence of ATP (1 mM), without Exo III; (c) in presence of Exo III (1 U/μL), without ATP; (d) in the presence of ATP (1 mM) and Exo III (1 U/μL). (C) Fluorescence spectra corresponding to the release of CPT upon treatment of 12-capped MP-SiO_2 NPs with variable concentrations of ATP in the presence of the Nb. BbvCI nicking enzyme (0.5 U/μL), for a fixed time interval of 90 min: (a) 0 μM; (b) 100 μM; (c) 500 μM; (d) 1 mM; (e) 2 mM. (D) Time-dependent fluorescence changes upon treatment of the CPT-loaded MP-SiO_2 NPs: (a) with no ATP and no nicking enzyme; (b) in the presence of only ATP (1 mM) without nicking enzyme; (c) in presence of nicking enzyme (0.5 U/μL) without ATP; (d) in the presence of ATP (1 mM) and nicking enzyme (0.5 U/μL).

units that are unlocked by biocatalytic processes (Exo III or Nb. BbvCI) was formulated as a general approach to control drug delivery and regulate cell death. Specifically, the high metabolic activity in cancer cells leads to high contents of ATP, and thus, it might provide a chemical trigger for the selective opening of the pores in cancer cells. The enhanced release of the chemotherapeutic drug, CPT, in the cancer cells are then anticipated to induce the superior death of cancer cells as compared to normal cells.

In a set of preliminary studies, we have examined the possible ATP-triggered release of CPT from the **11**-locked MP-SiO_2 NPs and the effect that the released CPT has on the death of the respective cells. In the first step, we examined the possible cytotoxicity of the MP-SiO_2 NPs on cells. The exterior surface of the DNA-locked NPs was functionalized with fluorescein isothiocyanate (FTIC) and MDA-MB-231 (breast cancer cells), and MCF-10a (normal breast cells) cells were subjected to the fluorescein-labeled NPs. Rapid endocytosis into the cells was observed, yet no cytotoxic effect was detected, Figure S7 (Supporting Information). In the next step, we made use of the report that EndoGI is present in cancer cells,[42] and it exhibits Exo III-type exonuclease activity. We loaded the MP-SiO_2 NPs with CPT and locked the drug in the pores with the ATP-sensitive hairpin **11**. MDA-MB-231 breast cancer cells and MCF-10a normal breast cells were subjected to the CPT-loaded MP-SiO_2 NPs. Figure 7 shows the fluorescence feature of the MDA-MB-231 cells, and the viability of the two types of cells after 48 h of treatment with the MP-SiO_2 NPs. Figure 7A shows the time-dependent fluorescence features of the MDA-MB-231 cells treated with the CPT-loaded NPs. The cells reveal green fluorescence after 24 h, corresponding to the fluorescein labels associated with the NPs, and this fluorescence prevails even after 48 h. This implies that the NPs are incorporated in the cells. The blue fluorescence, corresponding to unlocked CPT, is not observed after 24 h, reveals weak fluorescence after 30 h, and is

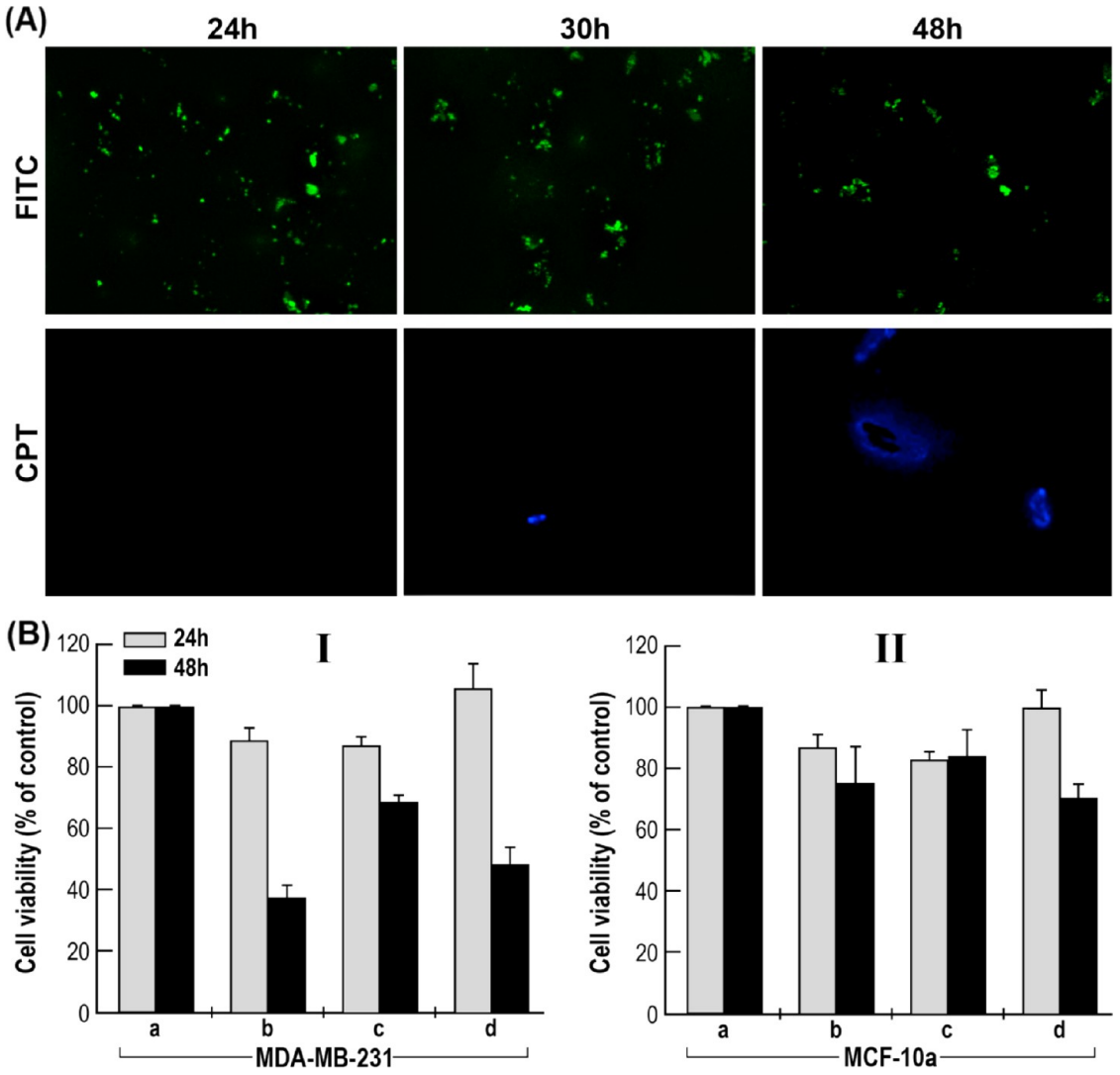

Figure 7. Cytotoxicity of CPT-MP-SiO_2 in breast cancer cells (MDA-MB-231) compared to normal breast cells (MCF-10a). (A) Epifluorescence microscopy images of the MDA-MB-231 breast cancer cells with endocytosed fluorescein isothiocyanate (FITC)-labeled and CPT-loaded MP-SiO_2 NPs at different time intervals (edocytosis was achieved by the treatment of the cell culture with 150 μg/mL of the silica NPs, see Experimental Section). Upper panel: green fluorescence of FITC, associated with the endocytosed particles. Lower panel: blue fluorescence of released CPT into the cells. (B) Cell viability results at two time intervals (24, 48 h) corresponding to MDA-MB-231 breast cancer cells (panel I) and normal MCF-10a breast epithelial cells (pane II): (a) cells nontreated with the CPT-loaded MP-SiO_2 NPs; (b) cells treated with the CPT-loaded MP-SiO_2 NPs; (c) cells treated with free CPT, 20 μg/mL; (d) cells pretreated with oligomycin, 25 μg/mL, and subsequently with the CPT-loaded MP-SiO_2 NPs.

intensified after a time interval of 48 h, implying that after this time interval CPT was released into the cells. Panels I and II of Figure 7B summarize the effect of the CPT-loaded NPs on the viability of the cells (Panel I, MDA-MB-231 breast cancer cells; Panel II, MCF-10a normal breast cells). Appropriate control systems are provided. From the results one may realize that *ca.* 65% of the cancer cells revealed cell death after 48 h, as compared to the CPT-nontreated control (entry a *vs* b), while only 25% of noncancerous cells experienced cell-death after this time interval (48 h). In a further control experiment, the two cell cultures were subjected to oligomycin, upon treatment with the CPT-loaded MP-SiO_2 NPs. Oligomycin acts as a suppressor of the ATPase synthesis of ATP,[43] and hence, the ATP-stimulated release of CPT in the cancer cells should be suppressed in the presence of oligomycin. Indeed, Figure 7B, panel I (compare entry b to d) reveals that in the presence of oligomycin only a 50% cell-death was observed as compared to 65% in the absence of the ATP synthesizing suppressor. These results are consistent with the fact that the high metabolic synthesis of ATP in the cancer cells leads to enhanced opening of the MP-SiO_2 NPs, and to the effective release of CPT that affects the cell death.

CONCLUSIONS

The present study has introduced a new capping and release mechanism of substrates entrapped in MP-SiO_2 NPs. The mechanism is based on tailored

nucleic acid caps that block the substrates in the pores of the NPs and the unlocking of the pores by analyte (biomarker)-induced rearrangements of the nucleic acid caps that undergo catalytic fragmentation in the presence of Exo III or a nicking enzyme. These coupled sensing/catalytic fragmentation processes lead to the regeneration of the analytes (biomarkers). The capping nucleic acid units recognize genes or molecular biomarkers through the formation of complementary duplex structures or aptamer–substrate complexes. The systems present sense-and-release nanostructures and a means to amplify the sensing process that releases the entrapped substrate by the regeneration of the analyte (biomarker). The biocatalytic process for releasing the substrate from the MP-SiO_2 NPs was then applied to stimulate the release of the anticancer drug, camptothecin, CPT, from the respective locked pores using nucleic acid or ATP as triggers for unlocking the pores in the presence of Exo III or the nicking enzyme, Nb. BbvCI. Since the metabolic synthesis of ATP is enhanced in cancer cells as compared to normal cells, and realizing that the biocatalyst EndoGI, exhibiting Exo III-type activities, is present in the cancer cells, the effects of the CPT-loaded MP-SiO_2 NPs locked with the ATP-dependent hairpin **11** on the viability of MDA-231 breast cancer cells and MCF-10a normal breast cells was examined. We demonstrated that after a time interval of 48 h, a 65% cell-death of the cancer cells was observed, where only 25% cell death was encountered with the normal cells. The higher CPT-induced death of the cancerous cells correlated well with the enhanced synthesis of ATP in the cancer cells. These preliminary results highlight the development of "smart" drug-loaded mesoporous nanoparticles that are unlocked and release the chemotherapeutic drug into target cancer cells by an intracellular biomarker (ATP). We believe that the study introduces a novel paradigm for cancer therapy.

EXPERIMENTAL SECTION

Materials. Tetraethyl orthosilicate (TEOS), (3-aminopropyl)-triethoxysilane (APTES) and rhodamine B (RhB) were purchased from Aldrich. *N*-(ε-Maleimidocaproyloxy)sulfosuccinimide ester (Sulfo-EMCS) was purchased from Pierce Biotechnologies. Hexadecyltrimethylammonium bromide (CTAB) and 4-(2-hydroxyethyl)piperazine-1-ethanesulfonic acid sodium salt (HEPES) were purchased from Sigma. Exonuclease III (Exo III), NEBuffer 1, nicking enzyme Nb. BbvCI and NEBuffer 2 were purchased from New England Biolabs. Camptothecin (CPT), oligomycin, adenosine 5′-triphosphate (ATP), uridine 5′-triphosphate (UTP), cytidine 5′-triphosphate (CTP) and guanosine 5′-triphosphate (GTP) were purchased from Sigma-Aldrich. All other chemicals used were of analytical grade and were used as received without any further purification. Ultrapure water from a NANOpure Diamond (Barnstead Int., Dubuque, IA) source was used throughout the experiments. All the DNA oligonucleotide sequences were purchased from Integrated DNA Technologies Inc. (Coralville, IA). The oligonucleotides were used as provided and diluted in aqueous solution.

The recognition site of the Nb. BbvCI nicking enzyme is as follows:

5′...CCTCAGC...3′
3′...GGAGT▲CG...3′

The sequences of the oligomers are as follows:
(**1**) 5′-$SH(CH_2)_6$ CAA GGG CAG AAG TCT TCA CTG CCC TTG CAC ACT-3′ Tm = 67.3 °C
(**2**) 5′-AGT GTG CAA GGG CAG TGA AGA CTT GAT TGT-3′
(**3**) 5′-AGT GTG CAA GAG CAG TGA AGA CTT GAT TGT-3′
(**4**) 5′-AGT GTG CTA GAG CAG TGA AGA CTT GAT TGT-3′
(**5**) 5′-AGT GTG CTA GAG CAG TTA AGA CTT GAT TGT-3′
(**6**) 5′-$SH(CH_2)_6$ AAC GAA GCT GAG GAT GTG TTC GTT-3′ Tm = 58.9 °C
(**7**) 5′-ATC CTC AGC TTC G-3′
(**8**) 5′-ATC CTG AGC TTC G-3′
(**9**) 5′-ATC ATG AGC TTC G-3′
(**10**) 5′-ATC ATG AGC GTC G-3′
(**11**) 5′-$SH(CH_2)_6$ CCT CCG CTA CCT GGG GGA GTA TTG CGG AGG AAG GTA-3′ Tm = 69.8 °C
(**12**) 5′-$SH(CH_2)_6$ CCT CCG CAA TAC TCC GCT GAG GCC TGG GGG AGT ATT GCG GAG GAA GGC CTC AGC-3′ Tm = 74.9 °C

Instruments. Fluorescence emission measurements were performed using a Cary Eclipse Device (Varian, Inc.). Rhodamine B (RhB) was excited at a wavelength of 554 nm. UV–vis absorption spectra were recorded with a Shimadzu UV-2401 spectrophotometer. TEM images were recorded on a Tecnai F20 G2 (FEI Co.) using an accelerating voltage of 200 kV. Surface areas were determined using a Nova 1200e Brunauer–Emmett–Teller (BET) meter (Quantachrome Instruments) by nitrogen adsorption/desorption at the temperature of liquid nitrogen.

Synthesis of Mesoporous Silica Nanoparticles (MP-SiO_2 NPs). Amino-functionalized MP-SiO_2 NPs were prepared according to a previously reported procedure.[30] The collected SiO_2 NPs were washed with large volumes of distilled water and ethanol using a centrifuge at 8000 rpm for 3 min. To remove the CTAB, the SiO_2 NPs were refluxed for 16 h in a solution composed of HCl (37%, 1.00 mL) and ethanol (80.00 mL). The obtained NPs were extensively washed with distilled water and ethanol. Finally, to remove the remaining solvent from the pores, the resulting, CTAB-free, amino-functionalized MP-SiO_2 NPs were placed in vacuum at 75 °C for 12 h.

Loading the Dye and Capping the Pores. To prepare monodispersed MP-SiO_2 NPs solution, 10 mg of silica NPs was placed into 950 μL of HEPES buffer (20 mM, pH 7.0) and sonicated for 30 min. The solution was reacted with 50 μL of sulfo-EMCS (10 mg/mL) and mixed for 30 min. To remove excess of EMCS, the MP-SiO_2 NPs were collected using a centrifuge at 8000 rpm for 3 min and redissolved in 950 μL of HEPES buffer (20 mM, pH 7.0). The purified SiO_2 NPs were reacted with the freshly reduced and purified thiolated oligonucleotides **1**, **6**, **11**, and **12** (80 μL, 1 mM). The resulting solution was mixed for 2 h, and the excess DNA was removed from the NPs solution by precipitation. The quantification of excess DNA that remained was accomplished by UV–vis spectroscopy in DNA/Exo III or DNA/nicking enzyme system and found to be 61 or 58 nmol, which corresponded to an amount of DNA immobilized to be 1.9 or 2.2 μmol/g SiO_2 NPs, respectively.

A water bath was used (90 °C) for the loading of the dye in the pores, in order to open the hairpin structure of the linked DNA. The purified MP-SiO_2 NPs were dissolved in 900 μL of HEPES buffer (20 mM, pH 7.0, containing 50 mM NaCl). 100 μL of RhB or CPT (10 mM) was added into the solution, and the reaction mixture was heated to 90 or 75 °C, respectively, using a water bath for 2 h under continuous stirring. Then, the sample was immersed separately in water bath at 75, 50, and 25 °C for 20 min under continuous stirring during the annealing process. Finally, the MP-SiO_2 NPs were washed at least seven times using distilled water, until a low background was achieved, to remove the physically adsorbed dye from the surface of the SiO_2 particles. The loading amount of RhB in DNA/Exo III or DNA/nicking enzyme systems was roughly calculated to be

37.8 or 31.3 μmol/g SiO_2 NPs, respectively. The loading amount of CPT in DNA/Exo III or DNA/nicking enzyme systems was calculated to be 34.5 or 28.6 μmol/g SiO_2 NPs, respectively.

Release of the Dye. To monitor the release of the dye in the two different systems, DNA/Exo III or DNA/nicking enzyme, the above-mentioned MP-SiO_2 NPs were suspended in 850 μL of distilled water and divided into five samples, each containing 160 μL of solution. Then, 20 μL of NEBuffer 1 and 10 μL of different concentration of Exo III, or 20 μL of NEBuffer 2 and 10 μL of different concentration of nicking enzyme were added into the resulting solution, respectively, and shaken gently. Finally, 10 μL of different concentrations of DNA were added into the mixture and shaken for 1 h, and then emitted fluorescence spectra of the samples were measured after precipitation.

To test the release of the dye in the ATP-stimulated Exo III or nicking enzyme system, the washed MP-SiO_2 NPs were dissolved in 850 μL of distilled water and divided into five samples, 160 μL each. The SiO_2 NPs were incubated with 20 μL of NEBuffer 1 and 10 μL of different concentration of Exo III, or 20 μL of NEBuffer 2 and 10 μL of different concentration of nicking enzyme, respectively. Then, 10 μL of different concentrations of ATP was added, the obtained solutions were shaken for 90 min, and the fluorescence spectra were measured after precipitation.

Effect of CPT on the Death of MDA-MB-231 (Breast Cancer), and MCF-10a (Normal Breast) Cells. MDA-MB-231 (breast cancer) and MCF-10a (normal breast) cells were planted at a density of 27 000 cells per well of 24-well tissue culture plates and left overnight. Subsequently, cells were preincubated with oligomycin (25 μg/mL) for 1 h, then loaded with MP-SiO_2 (150 μg/mL) twice (each loading lasted 3 h). Between the loadings cells were washed with fresh growth medium and then reloaded. Cells were further incubated overnight. To determine cell viability, 10 μL of alamar blue solution was added to each well of the plate, and the cells were placed in the CO_2 incubator for an additional 1 h. The fluorescence of alamar blue was checked in plate-reader (TECAN). The cells were cultured in glass-bottom microscope dishes and analyzed using an epifluorescence microscope, aided by confocal (quality equivalent) opti-grid device (Nikon TE 2000 microscope equipped with a thermostated stage and a Hamamatsu Orca-Era CCD camera) and driven by a Volocity 4 operating system (Improvision, Coventry, U.K.) that was used for both image data acquisition and analysis. Uptake of the NPs and release of CPT from the particles were measured microscopically with FITC-labeled (ex: 519 nm) and CPT-loaded (ex: 423 nm) NPs.

Conflict of Interest: The authors declare no competing financial interest.

Acknowledgment. This research is supported by NanoSensoMach ERC advanced Grant No. 267574 under the EC FP7/2007-2013 program. The research is performed under the auspices of the MINERVA Center for Biohybrid Complex Systems.

Supporting Information Available: SEM image of the MP-SiO_2 nanoparticles, N_2 adsorption−desorption isotherms and pore size distribution, a photograph of the nucleic acid functionalized MP-SiO_2 NPs before and after the loading with RhB, fluorescence measurements following the washing steps of the dyes from the channels of the SiO_2 NPs and the cytotoxicity of the SiO_2 NPs in MDA-MB-231 (breast cancer) and MCF-10a (normal breast) cells. This material is available free of charge *via* the Internet at http://pubs.acs.org.

REFERENCES AND NOTES

1. Slowing, I. I.; Vivero-Escoto, J. L.; Trewyn, B. G.; Lin, V. S.-Y. Mesoporous Silica Nanoparticles: Structural Design and Applications. *J. Mater. Chem.* **2010**, *20*, 7924–7937.
2. Jiao, F.; Frei, H. Nanostructured Cobalt Oxide Clusters in Mesoporous Silica as Efficient Oxygen-Evolving Catalysts. *Angew. Chem., Int. Ed.* **2009**, *48*, 1841–1844.
3. Huh, S.; Chen, H.-T.; Wiench, J. W.; Pruski, M.; Lin, V. S.-Y. Cooperative Catalysis by General Acid and Base Bifunctionalized Mesoporous Silica Nanospheres. *Angew. Chem., Int. Ed.* **2005**, *44*, 1826–1830.
4. Xiang, S.; Zhang, Y.; Xin, Q.; Li, C. Enantioselective Epoxidation of Olefins Catalyzed by Mn (salen)/MCM-41 Synthesized with a New Anchoring Method. *Chem. Commun.* **2002**, 2696–2697.
5. Vallet-Regi, M.; Balas, F.; Arcos, D. Mesoporous Materials for Drug Delivery. *Angew. Chem., Int. Ed.* **2007**, *46*, 7548–7558.
6. Zhao, Y.; Trewyn, B. G.; Slowing, I. I.; Lin, V. S.-Y. Mesoporous Silica Nanoparticle-Based Double Drug Delivery System for Glucose-Responsive Controlled Release of Insulin and Cyclic AMP. *J. Am. Chem. Soc.* **2009**, *131*, 8398–8400.
7. Liong, M.; Lu, J.; Kovochich, M.; Xia, T.; Ruehm, S. G.; Nel, A. E.; Tamanoi, F.; Zink, J. I. Multifunctional Inorganic Nanoparticles for Imaging, Targeting, and Drug Delivery. *ACS Nano* **2008**, *2*, 889–896.
8. Kim, J.; Kim, H. S.; Lee, N.; Kim, T.; Kim, H.; Yu, T.; Song, I. C.; Moon, W. K.; Hyeon, T. Multifunctional Uniform Nanoparticles Composed of a Magnetite Nanocrystal Core and a Mesoporous Silica Shell for Magnetic Resonance and Fluorescence Imaging and for Drug Delivery. *Angew. Chem., Int. Ed.* **2008**, *47*, 8438–8441.
9. Tsai, C.-P.; Hung, Y.; Chou, Y.-H.; Huang, D.-M.; Hsiao, J.-K.; Chang, C.; Chen, Y.-C.; Mou, C.-Y. High-Contrast Paramagnetic Fluorescent Mesoporous Silica Nanorods as a Multifunctional Cell-Imaging Probe. *Small* **2008**, *4*, 186–191.
10. Sakamoto, Y.; Kaneda, M.; Terasaki, O.; Zhao, D. Y.; Kim, J. M.; Stuckyk, G.; Shin, H. J.; Ryoo, R. Direct Imaging of the Pores and Cages of Three-Dimensional Mesoporous Materials. *Nature* **2000**, *408*, 449–453.
11. Liu, N.; Dunphy, D. R.; Atanassov, P.; Bunge, S. D.; Chen, Z.; Lopez, G. P.; Boyle, T. J.; Brinker, C. J. Photoregulation of Mass Transport through a Photoresponsive Azobenzene-Modified Nanoporous Membrane. *Nano Lett.* **2004**, *4*, 551–554.
12. He, D.; He, X.; Wang, K.; Cao, J.; Zhao, Y. A Light-Responsive Reversible Molecule-Gated System Using Thymine-Modified Mesoporous Silica Nanoparticles. *Langmuir* **2012**, *28*, 4003–4008.
13. Aznar, E.; Casasus, R.; Garcia-Acosta, B.; Marcos, M. D.; Martinez-Manez, R.; Sancenon, F.; Soto, J.; Amoros, P. Photochemical and Chemical Two-Channel Control of Functional Nanogated Hybrid Architectures. *Adv. Mater.* **2007**, *19*, 2228–2231.
14. Liu, R.; Zhao, X.; Wu, T.; Feng, P. Tunable Redox-Responsive Hybrid Nanogated Ensembles. *J. Am. Chem. Soc.* **2008**, *130*, 14418–14419.
15. Luo, Z.; Cai, K.; Hu, Y.; Zhao, L.; Liu, P.; Duan, L.; Yang, W. Mesoporous Silica Nanoparticles End-Capped with Collagen: Redox-Responsive Nanoreservoirs for Targeted Drug Delivery. *Angew. Chem., Int. Ed.* **2011**, *50*, 640–643.
16. Wan, X.; Wang, D.; Liu, S. Fluorescent pH-Sensing Organic/Inorganic Hybrid Mesoporous Silica Nanoparticles with Tunable Redox-Responsive Release Capability. *Langmuir* **2010**, *26*, 15574–15579.
17. Yang, Q.; Wang, S.; Fan, P.; Wang, L.; Di, Y.; Lin, K.; Xiao, F.-S. pH-Responsive Carrier System Based on Carboxylic Acid Modified Mesoporous Silica and Polyelectrolyte for Drug Delivery. *Chem. Mater.* **2005**, *17*, 5999–6003.
18. Gao, Q.; Xu, Y.; Wu, D.; Shen, W.; Deng, F. Synthesis, Characterization, and *in Vitro* pH-Controllable Drug Release from Mesoporous Silica Spheres with Switchable Gates. *Langmuir* **2010**, *26*, 17133–17138.
19. Zheng, H.; Wang, Y.; Che, S. Coordination Bonding-Based Mesoporous Silica for pH-Responsive Anticancer Drug Doxorubicin Delivery. *J. Phys. Chem. C* **2011**, *115*, 16803–16813.
20. Yu, A.; Wang, Y.; Barlow, E.; Caruso, F. Mesoporous Silica Particles as Templates for Preparing Enzyme-Loaded Biocompatible Microcapsules. *Adv. Mater.* **2005**, *17*, 1737–1741.
21. Park, C.; Kim, H.; Kim, S.; Kim, C. Enzyme Responsive Nanocontainers with Cyclodextrin Gatekeepers and Synergistic Effects in Release of Guests. *J. Am. Chem. Soc.* **2009**, *131*, 16614–16615.
22. Lei, C.; Shin, Y.; Liu, J.; Ackerman, E. J. Entrapping Enzyme in a Functionalized Nanoporous Support. *J. Am. Chem. Soc.* **2002**, *124*, 11242–11243.

23. Takahashi, H.; Li, B.; Sasaki, T.; Miyazaki, C.; Kajino, T.; Inagaki, S. Catalytic Activity in Organic Solvents and Stability of Immobilized Enzymes Depend on the Pore Size and Surface Characteristics of Mesoporous Silica. *Chem. Mater.* **2000**, *12*, 3301–3305.
24. Nguyen, T. D.; Tseng, H.-R.; Celestre, P. C.; Flood, A. H.; Liu, Y.; Stoddart, J. F.; Zink, J. I. A Reversible Molecular Valve. *Proc. Natl. Acad. Sci. U.S.A.* **2005**, *102*, 10029–10034.
25. Nguyen, T. D.; Liu, Y.; Saha, S.; Leung, K. C.-F.; Stoddart, J. F.; Zink, J. I. Design and Optimization of Molecular Nanovalves Based on Redox-Switchable Bistable Rotaxanes. *J. Am. Chem. Soc.* **2007**, *129*, 626–634.
26. Zhu, C.-L.; Lu, C.-H.; Song, X.-Y.; Yang, H.-H.; Wang, X.-R. Bioresponsive Controlled Release Using Mesoporous Silica Nanoparticles Capped with Aptamer-Based Molecular Gate. *J. Am. Chem. Soc.* **2011**, *133*, 1278–1281.
27. Hou, X.; Guo, W.; Xia, F.; Nie, F.-Q.; Dong, H.; Tian, Y.; Wen, L.; Wang, L.; Cao, L.; Yang, Y.; *et al.* A Biomimetic Potassium Responsive Nanochannel: G-Quadruplex DNA Conformational Switching in a Synthetic Nanopore. *J. Am. Chem. Soc.* **2009**, *131*, 7800–7805.
28. Xia, F.; Guo, W.; Mao, Y.; Hou, X.; Xue, J.; Xia, H.; Wang, L.; Song, Y.; Ji, H.; Ouyang, Q.; *et al.* Gating of Single Synthetic Nanopores by Proton-Driven DNA Molecular Motors. *J. Am. Chem. Soc.* **2008**, *130*, 8345–8350.
29. He, X.; Zhao, Y.; He, D.; Wang, K.; Xu, F.; Tang, J. ATP-Responsive Controlled Release System Using Aptamer-Functionalized Mesoporous Silica Nanoparticles. *Langmuir* **2012**, *28*, 12909–12915.
30. Chen, C.; Pu, F.; Huang, Z.; Liu, Z.; Ren, J.; Qu, X. Stimuli-Responsive Controlled-Release System Using Quadruplex DNA-Capped Silica Nanocontainers. *Nucleic Acids Res.* **2011**, *39*, 1638–1644.
31. Zhang, Y.; Yuan, Q.; Chen, T.; Zhang, X.; Chen, Y.; Tan, W. DNA-Capped Mesoporous Silica Nanoparticles as an Ion-Responsive Release System to Determine the Presence of Mercury in Aqueous Solutions. *Anal. Chem.* **2012**, *84*, 1956–1962.
32. He, D.; He, X.; Wang, K.; Cao, J.; Zhao, Y. A Photon-Fueled Gate-Like Delivery System Using i-Motif DNA Functionalized Mesoporous Silica Nanoparticles. *Adv. Funct. Mater.* **2012**, *22*, 4704–4710.
33. Yuan, Q.; Zhang, Y.; Chen, T.; Lu, D.; Zhao, Z.; Zhang, X.; Li, Z.; Yan, C.-H.; Tan, W. Photon-Manipulated Drug Release from a Mesoporous Nanocontainer Controlled by Azobenzene-Modified Nucleic Acid. *ACS Nano* **2012**, *6*, 6337–6344.
34. Chen, C.; Geng, J.; Pu, F.; Yang, X.; Ren, J.; Qu, X. Polyvalent Nucleic Acid/Mesoporous Silica Nanoparticle Conjugates: Dual Stimuli-Responsive Vehicles for Intracellular Drug Delivery. *Angew. Chem., Int. Ed.* **2011**, *50*, 882–886.
35. Zhang, Z.; Balogh, D.; Wang, F.; Willner, I. Smart Mesoporous SiO_2 Nanoparticles for the DNAzyme-Induced Multiplexed Release of Substrates. *J. Am. Chem. Soc.* **2013**, *135*, 1934–1940.
36. Freeman, R.; Liu, X.; Willner, I. Amplified Multiplexed Analysis of DNA by the Exonuclease III-Catalyzed Regeneration of the Target DNA in the Presence of Functionalized Semiconductor Quantum Dots. *Nano Lett.* **2011**, *11*, 4456–4461.
37. Liu, X.; Aizen, R.; Freeman, R.; Yehezkeli, O.; Willner, I. Multiplexed Aptasensors and Amplified DNA Sensors Using Functionalized Graphene Oxide: Application for Logic Gate Operations. *ACS Nano* **2012**, *6*, 3553–3563.
38. Liu, X.; Freeman, R.; Willner, I. Amplified Fluorescence Aptamer-Based Sensors Using Exonuclease III for the Regeneration of the Analyte. *Chem.—Eur. J.* **2012**, *18*, 2207–2211.
39. Weizmann, Y.; Beissenhirtz, M. K.; Cheglakov, Z.; Nowarski, R.; Kotler, M.; Willner, I. A Virus Spotlighted by an Autonomous DNA Machine. *Angew. Chem., Int. Ed.* **2006**, *45*, 7384–7388.
40. Beissenhirtz, M. K.; Elnathan, R.; Weizmann, Y.; Willner, I. The Aggregation of Au Nanoparticles by an Autonomous DNA Machine Detects Viruses. *Small* **2007**, *3*, 375–379.
41. Shlyahovsky, B.; Li, D.; Weizmann, Y.; Nowarski, R.; Kotler, M.; Willner, I. Spotlighting of Cocaine by an Autonomous Aptamer-Based Machine. *J. Am. Chem. Soc.* **2007**, *129*, 3814–3815.
42. Temme, C.; Weissbach, R.; Lilie, H.; Wilson, C.; Meinhart, A.; Meyer, S.; Golbik, R.; Schierhorn, A.; Wahle, E. The Drosophila Melanogaster Gene Cg4930 Encodes a High Affinity Inhibitor for Endonuclease G. *J. Biol. Chem.* **2009**, *284*, 8337–8348.
43. Devenish, R. J.; Prescott, M.; Boyle, G. M.; Nagley, P. The Oligomycin Axis of Mitochondrial ATP Synthase: OSCP and the Proton Channel. *J. Bioenerg. Biomembr.* **2000**, *32*, 507–515.